HHS Public Access

Author manuscript

IEEE Trans Ultrason Ferroelectr Freq Control. Author manuscript; available in PMC 2017 September 01.

Published in final edited form as:

IEEE Trans Ultrason Ferroelectr Freq Control. 2016 September ; 63(9): 1276–1287. doi:10.1109/TUFFC.2016.2539323.

On the Quantitative Potential of Viscoelastic Response (VisR) Ultrasound Using the One-Dimensional Mass-Spring-Damper Model

Mallory R. Selzo, **Christopher J. Moore**, **Md Murad Hossain**, **Mark L. Palmeri [Member, IEEE]**, and **Caterina M. Gallippi [Member, IEEE]**

Abstract

Viscoelastic Response (VisR) ultrasound is an acoustic radiation force (ARF)-based imaging method that fits induced displacements to a one-dimensional (1D) mass-spring-damper (MSD) model to estimate the ratio of viscous to elastic moduli, τ, in viscoelastic materials. Error in VisR τ estimation arises from inertia and acoustic displacement underestimation. These error sources are herein evaluated using finite element method (FEM) simulations, error correction methods are developed, and corrected VisR τ estimates are compared to true simulated τ values to assess VisR's relevance to quantifying viscoelasticity. In regards to inertia, adding a mass term in series with the Voigt model, to achieve the MSD model, accounts for inertia due to tissue mass when ideal point force excitations are used. However, when volumetric ARF excitations are applied, the induced complex system inertia is not described by the single-degree-of-freedom MSD model, causing VisR to overestimate τ. Regarding acoustic displacement underestimation, associated deformation of ARF-induced displacement profiles further distorts VisR τ estimates. However, median error in VisR τ is reduced to approximately −10% using empirically derived error correction functions applied to simulated viscoelastic materials with viscous and elastic properties representative of tissue. The feasibility of corrected VisR imaging is then demonstrated in vivo in the rectus femoris muscle of an adult with no known neuromuscular disorders. These results suggest VisR's potential relevance to quantifying viscoelastic properties clinically.

Keywords

Acoustic Radiation Force; Mass-Spring-Damper; Viscoelasticity; Viscoelastic Response (VisR) Ultrasound

I. Introduction

The viscoelastic properties of tissue have been shown to be relevant to diagnosing and monitoring disease. For example, ultrasound and magnetic resonance-based techniques have interrogated the viscoelastic properties of tissue to detect diseases of the liver [1]–[4], malignant tumors [5], [6], and skeletal muscle composition [7]–[9], among other diseases. One approach to viscoelastic property assessment by ultrasound involves using acoustic

Send Correspondence to: cmgallip@email.unc.edu.

radiation force (ARF) to induce compressive and shear waves at depth in tissue, and the associated dynamic tissue deformations are monitored and related to viscoelasticity. Shear wave dispersion (as in Shearwave Dispersion Ultrasound Vibrometry (SDUV) [10] and Shear Wave Spectroscopy[2]), shear wave attenuation [11], [12], and tissue creep behavior (as in Kinetic Acoustic Vitreoretial Examination (KAVE) [13], Monitored Steady-State Excitation Recovery (MSSER) [14], ARF Creep imaging [15], hybrid creep with SDUV [16] and Viscoelastic Response (VisR) imaging [9]) have been exploited to estimate the viscoelastic parameters of tissue using ARF.

VisR imaging is performed by applying two consecutive ARF impulses, separated by < 1 ms in time and delivered to the same region of excitation, and monitoring induced displacements in the region of excitation. VisR then fits the ultrasonically tracked displacements to the one-dimensional (1D) mass-spring-damper (MSD) model to estimate the material relaxation time constant, τ, given by the ratio of viscosity to elasticity. VisR has previously been demonstrated for qualitatively assessing the viscoelastic properties of materials using the 1D first-order Voigt model, which supported discrimination of features in tissue-mimicking phantoms and in muscle [9]. However, VisR's relevance to quantifying viscoelasticity is under investigation. The purpose of this manuscript is to identify, evaluate, and minimize sources of error in VisR τ calculations.

A prominent source of error in VisR τ calculations is inertia, or the tendency of a body with mass to resist any change in its motion [17]. In the previous VisR description [9], inertia was neglected because τ was estimated by fitting displacement profiles to the Voigt model, a lumped spring and dashpot system that assumes a massless material [18]. However, in reality, all biological tissue has mass. The mass density of most soft tissues is slightly higher than that of water, typically lying in the range of 1.00–1.07 g/cm3 [19]. In ARF applications, inertia will manifest as a delay in the time it takes for the material to reach its peak displacement and an increase in time needed to recover [20]. When inertial effects are ignored, these changes in the response of the material will be interpreted as an increase in the viscosity and/or a decrease in the stiffness of the material, both of which will result in a false increase in VisR τ.

If the ARF excitation was an ideal point force, such that only a small focal region caused inertial effects, a potential solution to accounting for inertia would involve fitting measured displacements to a lumped parameter MSD model that places a mass term in series with the Voigt model [13]. VisR performance using the MSD verses the conventional Voigt model is herein compared through finite element method (FEM) modeling of point force-induced dynamics. Each model's capacity to describe the deformation caused by a point force and to enable VisR τ measurement in viscoelastic materials is evaluated.

While an ARF excitation may be modeled as an ideal point force, in reality, ARF generated by conventional ultrasound transducers is volumetric and spans millimeters in axial, lateral and elevation dimensions, as depicted in Fig. 1(a). The three-dimensional nature of the ARF excitation induces displacement in tissue extending beyond the tracking focal region, and the complex system inertia is not accurately accounted for by a single degree of freedom (SDF) model such as the MSD, as demonstrated by Zhao and Pelegri [15]. The unaccounted

complex system inertia extends the duration of the force experienced at the tracking focus beyond that of the applied ARF excitation. Illustrated in Fig. 1(b), the volumetric force prolongs the displacement and recovery behavior of the material, falsely indicating lower elasticity and/or higher viscosity, and causing VisR to overestimate τ.

Correcting VisR's τ overestimation due to the volumetric nature of the ARF excitation could be achieved by fitting displacements to a multiple degree of freedom (MDF) model, with associated mathematical complexities. Alternatively, the modeled forcing function could be modified to incorporate inertial forces, but this would require a priori knowledge of the complex system inertia, which is materially and geometrically dependent and generally unknown. Instead, a priori material estimates are obviated herein by correcting VisR τ overestimation using empirically determined correction functions.

A second source of error in VisR τ calculations is acoustic displacement underestimation [21], [22]. For VisR imaging performed using one-dimensional linear array transducers, measured displacement profiles will be underestimated, with displacements measured shortly after the ARF excitation more severely underestimated than those measured later after the excitation. The net impact is that the shape of the acoustically tracked displacement profile is distorted in such a manner that falsely reflects τ. As is the case for the volumetric forcing function, the degree of error in VisR τ calculations caused by acoustic displacement underestimation is materially dependent, with stiffer materials experiencing less displacement underestimation and therefore less displacement profile distortion. Again, rather than relying on a priori material property estimates to attempt to reverse acoustic displacement underestimation, empirically determined correction functions are generated to correct for acoustic displacement underestimation. For simplicity, combined correction functions, which adjust VisR τ calculations to account for both the volumetric nature of the ARF excitation and acoustic displacement underestimation, are derived.

The relevance of this approach to VisR τ error correction is evaluated using finite element method (FEM) simulations and demonstrated in vivo in human rectus femoris muscle. By extending VisR to account for inertia, including that imposed by volumetric ARF excitations, and acoustic displacement underestimation, this manuscript demonstrates VisR's potential and limitations for quantifying τ in viscoelastic materials.

II. Background

The mass-spring-damper (MSD) model describes the viscoelastic properties of a material while accounting for mass by placing an inertial component in series with the Voigt model [13], [23]. A schematic for the MSD model is shown in Fig. 2(a). The governing dynamics for an MSD model are given by the second order, non-homogeneous differential:

$$m\frac{d^2}{dt^2}u(t)+\eta\frac{d}{dt}u(t)+\mu u(t)=F(t) \quad (1)$$

where F(t) is the applied force, u(t) is the displacement, μ is the elastic constant of the spring, η is the coefficient of viscosity of the damper, and m is the effective mass of the

system. If the ARF excitation is described in time as a rectangular function of force magnitude A and duration t_{ARF}, then the two ARF excitations used for VisR can be described as two rectangular pulses of duration t_{ARF} and amplitude A, and separated by t_s in time, as illustrated in Fig. 2(b) and defined as:

$$F(t)=A\left(H(t)-H(t-t_{ARF})\right)+A(H(t-t_{ARF}-t_s)-H(t-2t_{ARF}-t_s)) \quad (2)$$

where $H(t)$ is the unit Heaviside function. Substituting (2) into (1) yields:

$$\frac{d^2}{dt^2}u(t)+\omega^2\tau\frac{d}{dt}u(t)+\omega^2u(t)=S\omega^2\left(H(t)-H(t-t_{ARF})-H(t-t_{ARF}-t_s)+H(t-2t_{ARF}-t_s)\right) \quad (3)$$

where ω is the natural frequency, **τ** is the relaxation time constant, and S is the static sensitivity of the system. These material parameters may be defined in terms of the properties of the medium and the amplitude of the applied force as:

$$\omega=\sqrt{\frac{\mu}{m}};\tau=\frac{\eta}{\mu};S=\frac{A}{\mu}. \quad (4)$$

Equation (3) can be solved for displacement and fit to the observed VisR displacement versus time profile to obtain estimates of ω, **τ**, and S. Note that while previous implementations of VisR solved for **τ** explicitly [9], this approach estimates ω, **τ**, and S by fitting measured displacement profiles to (3) using non-linear least-squares minimization. When considering the relevance of the MSD model to describing the mechanical properties of tissue, one must recognize that, in reality, tissue is not a system of well-defined, separate moving parts. Rather, tissue consists of a continuously spread mass and geometry in a distributed system. Such continuum, or distributed parameter, systems have infinite number of resonant frequencies and corresponding displacement dynamics. However, by discretizing the system into a meshwork of interconnected systems in three dimensions with multiple degrees of freedom, the system's overall behavior may be approximated using the FE method.

More specifically, FEM software models a continuum system as a meshwork of distributed masses, springs and dampers oriented in three-dimensions. In this manner, the modeled MDF system is described as:

$$\boldsymbol{M}\ddot{\boldsymbol{u}}+\boldsymbol{B_d}\dot{\boldsymbol{u}}+\boldsymbol{E}_s\boldsymbol{u}=\boldsymbol{f_e} \quad (5)$$

where $\boldsymbol{f_e}$ is the matrix of force inputs associated with each mass, $\boldsymbol{u}$ is a vector containing the displacement coordinates for each degree of freedom, $\boldsymbol{E}_s$ is the matrix of elastic constants of

the springs, $\boldsymbol{B_d}$ is the matrix of viscosity coefficients of the dampers, and $\boldsymbol{M}$ is the system mass matrix. Constant matrices $\boldsymbol{E_s}$, $\boldsymbol{B_d}$, and $\boldsymbol{M}$ have dimension N×N, where N is the number of degrees of freedom in the model. Note that equation (5) has a form similar to that of (1). In effect, FEM vibration analysis discretizes a continuous structure and its geometry into finite portions, called ‘elements,’ such that the continuously distributed system is modeled as a field of independent, but connected systems with hundreds to thousands to millions of degrees of freedom overall.

While FEM analysis models tissue as a MDF system, the MSD model describes only a SDF [15]. Thus, the fundamental assumptions associated with applying the MSD model to describing the viscoelastic properties of tissue are that: 1) the induced motion is highly localized, 2) the tissue response reflects only the local distribution of mechanical properties, and 3) the tissue is homogeneous. Importantly, these assumptions break down in the context of the volumetric nature of ARF excitations due to the associated complex and interrelated three-dimensional system inertia they induce [15]. In tissue (and in FE simulation) the system inertia arises from complex interactions of both compressive and shear dynamics; however, the MSD model accounts for only uniaxial displacements from compressive stresses, neglecting shear phenomena. Therefore, without correction, VisR estimates of ω, τ, and S do not reflect the true material properties but rather a set of *effective* material properties that are influenced by the complex system inertia. As described in the Introduction, we herein evaluate VisR τ correction, with and without the confounding effects of acoustic displacement underestimation [21], [22], using correction functions empirically determined from estimated ω and τ parameters in homogeneous media.

III. Methods

A. Inertial Compensation with Point Force Excitation in FEM Simulation

The purpose of this portion of the simulation study was to evaluate inertial compensation in VisR performed using idealized point force ARF excitations. Thus, the excitation was modeled as a concentrated force on a single node at a given focal depth, and VisR τ was calculated directly from the FEM modeled displacements. Mass, and thereby the degree of inertia, was varied by altering the density of the modeled materials.

The employed finite element method (FEM) models were adapted from those previously developed by Palmeri et al. for investigating the response of an elastic material to an ARF excitation [25]. A three-dimensional, rectangular, solid mesh was assembled from 0.5 mm, cubic elements using LS-PREPOST (Livermore Software Technology Corp., Livermore, CA). The mesh extended 5 mm in elevation, 7.5 mm laterally, and 40 mm axially. A 5 elements thick, perfectly matched layer (PML) was added to the exterior boundaries of the mesh to absorb any waves generated during the simulation and ensure that they were not reflected back into the region of interest (ROI) [26]. As a requirement of the PML, all nodes on outer faces were fully constrained. Quarter-symmetry was assumed in both the lateral and elevation dimensions, requiring only a quarter of the field to be modeled, and thus reducing the computational requirements of the simulation.

Tissue was modeled as a viscoelastic material using the MAT_KELVIN-MAXWELL_VISCOELASTIC material model provided with the commercially available FEM solver, LS- DYNA (Livermore Software Technology Corp., Livermore, CA). The Young's modulus of the material was varied from 10 to 50 kPa, by steps of 10 kPa, and the viscous coefficient was varied from 3 to 7 Pa·s, by steps of 2 Pa·s. This produced 15 different viscoelastic materials with τ values ranging from 0.06 ms to 0.70 ms. The MAT_PML_ELASTIC material model was employed for the PML, with the elasticity set to match that of the corresponding viscoelastic material. The density of the simulated materials was varied from nearly massless at 0.05 g/cm^3 to a physiologically relevant value of 1.0 g/cm^3. Note that this wide variation in density goes beyond the typical tissue range of 1.00–1.07 g/cm^3. Recall that the purpose of manipulating density in this manner was not to recapitulate the density of tissue but rather to enable direct evaluation of the impact of mass (inertia) on VisR τ calculations. A Poisson's ratio of 0.499 was used for all simulations.

As described above, displacement was induced using a concentrated point force on the single node centered laterally and elevationally within the mesh and at an axial depth of 25 mm. The temporal extent of the force was described according to (2) to simulate two, 300-cycle ARF excitations at 4.21 MHz (t_{ARF} = 71 μs), separated by 4 ms in time (t_s=0.4 ms). This time separation was selected to allow for partial recovery of the material between successive ARF excitations.

The FEM simulations were performed using LS-DYNA, using an explicit, time-domain integration method. For each simulation, a dataset describing the axial displacements at the focal node was obtained. Axial displacement versus time profiles were fit to the Voigt and MSD models by nonlinear regression using the Nelder-Mead algorithm [27], via a custom C ++ implementation, to solve for τ from FE displacements.

VisR τ estimates from Voigt and MSD models were statistically compared to the true ratios of viscous to elastic moduli of the materials using the Wilcoxon rank-sum two-sample test. A p value of < 0.05 was defined as significant.

B. Inertial Compensation with Volumetric ARF Excitation in FEM Simulation

The purpose of this part of the simulation study was to evaluate the impact of the volumetric nature of the ARF excitations and the associated complex three-dimensional system inertia on VisR τ calculations. Thus, ARF excitations were modeled as three-dimensional body forces, and VisR τ was calculated directly from the FEM modeled displacements measured at the node positioned at 25 mm axially, centered laterally and elevationally in the ARF excitation.

A solid mesh was generated as described above, spanning 4 mm in elevation, 10 mm laterally, and 45 mm axially and consisting of 0.25 mm cubic elements. Elasticity of the modeled viscoelastic materials was varied from 5 to 100 kPa in steps of 5 kPa, and viscosity was varied from 0.5 to 9.5 Pa·s in steps of 1 Pa·s, for a total of 200 materials with τ values ranging from 0.005 ms to 1.900 ms. Then, an additional set of 20 viscoelastic materials was generated, with elasticity ranging from 5 to 100 kPa, each with random viscosity in the

range of 1.0 to 9.0 Pa·s and τ values in the range of 0.010 ms to 1.800 ms. A density of 1.0 g/cm^3 and a Poisson's ratio of 0.499 were used for all materials.

Field II [28] was used to simulate the acoustic intensity fields associated with a Siemens VF7-3 linear array transducer (Siemens Medical Solutions USA, Inc., Ultrasound Division). The transducer was simulated as transmitting at 4.21 MHz, with a lateral focal configuration of F/1.5, and a lateral focal depth of 25 mm. This corresponds to the experimental setup typically utilized to perform VisR ultrasound.

Three-dimensional intensity fields were computed, normalized, and scaled to a peak, pulse-average intensity value of 1000 W/cm^2. The intensity field was converted to radiation body force values by assuming a tissue attenuation of 0.5dB/cm/MHz and a 1540 m/s speed of sound, and using the following equation:

$$\vec{F} = \frac{2\alpha \vec{I}}{c} \quad (6)$$

where α and c are the absorption coefficient and speed of sound in the medium, respectively, and I is the spatially-varying, scaled intensity [29], [30]. Nodal point loads were computed by concentrating the body force contributions over an element volume and oriented in the axial direction as demonstrated in Fig. 1(a).

For each simulation, a dataset describing the axial displacements was generated, and values of τ, ω, and S were obtained from the MSD fit to displacement at the center node at 25 mm via Nelder-Mead minimization.

C. Incorporation of Acoustic Displacement Underestimation

To evaluate the impact of acoustic displacement underestimation on VisR τ calculations, the simulation data generated as described in section B was subjected to simulated acoustic tracking, and VisR was performed using the acoustically tracked data. The method of simulating ultrasound imaging of ARF-induced dynamics and subsequently adding decorrelation was adapted from Palmeri et al [25]. First, a three-dimensional Field II scatterer phantom with fully-developed speckle (11 scatterers per resolution cell) was defined to span the volume of the FEM mesh with added symmetry quadrants. Next, nodal displacements output by LS-DYNA were loaded into MATLAB (Mathworks Inc., Natick, MA) and used to linearly-interpolate scatterer positions for every time step in the ARFI ensemble. After generating the scatterer-position matrices for each time step in the ARFI ensemble, the corresponding RF lines were simulated using Field II and motion tracked using one-dimensional normalized cross correlation [31]. A total of 10 independent scatter realizations were used. Then, for each pixel, the mean displacement profile from each of the 10 scatter realizations was fit to the MSD model to solve for VisR τ in the presence of acoustic displacement underestimation.

D. Derivation of Error Correction Functions

VisR τ correction functions were empirically determined as functions of estimated ω and τ that minimized median absolute percent error between corrected VisR and true τ for the 220 modeled materials. Multiple functions were derived to account for error caused by complex system inertia, as well as inertia coupled with acoustic displacement underestimation. Fig. 3 illustrates a flow diagram describing the process of deriving error correction functions. First, the 220 simulated viscoelastic materials were randomly divided into two sets: training/validation (n=170 materials) and test (n=50 materials). Second, for the materials in the training/validation set, the material τ values were plotted (Fig. 4) as a function of VisR estimated τ and ω values. The resulting 3D surface was fit (Table Curve 3D, Systat, Inc., San Jose, CA) to over 3000 linear and nonlinear equations to determine 50 possible error models that utilized the minimum number of parameters (e.g. simplest model possible) while maximizing the model fit (R^2). Third, K-fold cross validation, with K = 5 [32], was performed to determine the coefficients of the 50 possible error models by minimizing absolute median percent error (AMPE). In this manner, the distribution of the 170 materials across training (136 materials) and validation (34 materials) assignments was randomly determined five times to derive five possible sets of coefficients for each of the 50 possible error models. Fourth, K-fold coefficient determination was repeated 50 times with unique seeds, such that different materials were assigned to training and validation sets with each iteration, to generate a total of 5 × 50 = 250 possible sets of coefficients for each of the 50 possible error models. Fifth, the best coefficient set for each of the 50 possible error models was selected based on the minimum AMPE in the validation set materials. More specifically, the AMPE in the 36 validation materials was calculated for each of the 250 iterations on the validation set composition, and the set of coefficients yielding the minimum AMPE was identified for each of the 50 possible error models. Sixth, the resulting 50 error correction functions, each with its best coefficients, were then applied to the test set, which was never part of the training or validation sets. Finally, the error correction function and set of coefficients that yielded the minimum AMPE in the test set was identified.

For the FEM simulated data using the volumetric ARF excitation but neglecting acoustic displacement underestimation, the inertial error correction function for VisR τ estimates at the 25 mm focal depth was determined to be of the form:

$$\tau_{\text{corrected}} = a + b * \omega_{\text{VisR}} + c * \tau_{\text{VisR}}^{d} \quad (7)$$

where a, b, c and d are coefficients; ω_{VisR} and τ_{VisR} are the estimates of ω, and τ from the MSD model fit. The coefficient values of for this equation were determined to be:

$$a = 0.0610, b = -0.0070, c = 0.2562, d = 1.4806 \quad (8)$$

Because the ARF distribution, and thus the associated three-dimensional system inertia, changes with axial distance from the focus, a separate correction function was uniquely

derived using the process outlined in Fig. 3 for a depth 5 mm below the focal depth, yielding the inertial correction function for a focal depth of 30 mm:

$$\tau_{\text{corrected}} = a + b * \omega_{\text{VisR}}^2 + \frac{c}{\omega_{\text{VisR}}^2} \quad (9)$$

with coefficient values:

$$a = 0.2434, b = -0.0049, c = 0.6577. \quad (10)$$

Similarly for the ultrasonically tracked FE data, which is subject to error from both complex inertia and acoustic displacement estimation, the correction function at the 25 mm focal depth was determined to have the form:

$$\tau_{\text{corrected}} = a + b * \tau_{\text{VisR}} + \frac{c}{\omega_{\text{VisR}}} + \frac{d}{\omega_{\text{VisR}}^2} \quad (11)$$

with optimal coefficient values

$$a = -0.0636, b = -0.3887, c = 1.8689, d = 0.5186. \quad (12)$$

For the ultrasonically tracked data 5 mm below the focus (30 mm), the error correction function was determined as:

$$\tau_{\text{corrected}} = a + b * \tau_{\text{VisR}} + \frac{c * \ln(\omega_{\text{VisR}})}{\omega_{\text{VisR}}} \quad (13)$$

with coefficient values:

$$a = 0.2087, b = 0.2749, c = -1.0320. \quad (14)$$

E. In Vivo Demonstration in Human Rectus Femoris Muscle

To demonstrate its clinical feasibility and potential relevance, VisR imaging was performed in the rectus femoris muscle of a healthy adult female with no known neuromuscular disorders. VisR was implemented using a Siemens Acuson Antares Scanner, specially equipped for research purposes, and a VF7-3 linear array transducer (Siemens Medical Solutions, USA Inc. Ultrasound Division). The VisR beam sequence included two 300-cycle ARF excitations at 4.21 MHz with F/1.5 focal configuration, with the two excitations separated by 0.4 ms in time and delivered to the same region of excitation. The excitations were preceded, separated, and followed by two-cycle motion tracking lines centered at 6.15

MHz with an F/1.5 lateral focal configuration for a total 4.4 ms ensemble length. The imaging focal depth was 25 mm.

A total of 40 lateral locations were acquired for two-dimensional imaging, and image acquisitions were repeated three times, without moving the transducer position. Resulting acoustically-tracked displacement profiles measured at each pixel across the two-dimensional field of view were linearly motion filtered [33] and then fit to the MSD model. VisR τ estimates at depths ranging from 23 to 28 mm and 28 to 33 mm were corrected using (11–12) and (13–14), respectively. Median and standard deviation (std) of τ values were computed by first finding the median τ value in the depth range of 23 to 33 mm for each of 40 lateral lines in each of three repeated acquisitions. Then, the median and standard deviation of these 120 median τ values (1 median τ values per lateral line × 40 lateral lines per image × 3 repeated image acquisitions) was calculated. Parametric images of uncorrected and corrected VisR τ were rendered and superimposed on the corresponding B-Mode image for anatomical reference.

IV. Results

A. Inertial Compensation with Point Force Excitation in FEM Simulation

Representative displacement profiles in the 20 kPa, 5 Pa·s simulated material are shown in Fig. 5 for densities of (panel a) 0.05 g/cm^3 and (panel b) 1.0 g/cm^3. Recall that while a density of 0.05 g/cm^3 is not representative of real tissue, a range of low- to high-density viscoelastic materials are modeled to evaluate the impact of mass on VisR performance. The fitted Voigt and MSD models are shown as blue and green dotted lines, respectively, while the FEM displacement is displayed in red. The accuracy of the model in describing the dynamics of the deformation was determined by the closeness of fit between the FEM simulated displacement and the model predicted displacement, given by the mean squared error (MSE) statistic. For the 0.05 g/cm^3 density material, the MSE of the Voigt fit was 0.0029 μm^2 and the MSE of the MSD model fit was 0.00044 μm^2. In the 1.0 g/cm^3 density material, the MSE increased by 200 times to 0.5794 μm^2 when fitting with the Voigt model and by 1.7 times to 0.00075 μm^2 when fitting with the MSD model.

Fig. 6 shows the VisR τ estimates in all 15 viscoelastic materials plotted against the simulated material τ when the density of the materials was (panels a–b) 0.05 g/cm^3 and (panels c–d) 1.0 g/cm^3. Using the Voigt model, τ estimates were not significantly ($p = 1.0$) different from the programmed material τ values when the density was 0.05 g/cm^3 (panel a); however, when density was increased to 1.0 g/cm^3 the Voigt model produced τ estimates that were significantly larger ($p<0.001$) than the true τ of the material (panel c). For both 0.05 (panel b) and 1.0 g/cm^3 (panel d), the MSD model generated τ values that were consistent with the material τ values ($p=1.0$ and $p=0.9$, respectively). The p-values testing the null hypothesis that the VisR-derived τ values are consistent with the modeled material are illustrated versus material density for the Voigt and MSD model fits in Fig. 7.

B. Inertial Compensation with Volumetric ARF Excitation in FEM Simulation

Fig. 8 shows uncorrected and inertia-corrected VisR τ estimates from FEM displacements versus true material τ value for the 50 test materials. The ARF focal depth is 25 mm, and the displayed VisR τ estimates were measured at 25 mm (panels a–b) or 30 mm (panels c–d) in depth. Recall that for these axial depths two different correction functions were generated, as described in section III.D, such that the VisR τ estimates at 25 mm were corrected using (7) and (8), and VisR τ estimates at 30 mm were corrected using (9) and (10). Panels (a) and (c) show that, for both 25 and 30 mm depth positions, uncorrected VisR τ values are statistically significantly larger than the true material τ values ($p<0.001$ for both depths). After inertial correction, panels (b) and (d) illustrate that VisR and true material τ values are not statistically significantly different ($p = 0.95$ and $p = 0.94$, respectively), with comparable corrected performance at the two depth positions. Table 1 summarizes error metrics for these data. Before inertial correction, median (inter-quartile range) percent error at 25 and 30 mm depth positions was 333.7 (375.8)% and 525.7 (523.5)%, respectively; however, after correction, median (inter-quartile range) percent error was reduced to −9.3 (25.7)% and −9.6 (42.7)%.

C. Inertial Compensation and Acoustic Displacement Underestimation Correction in FEM Simulation

Fig. 9 similarly shows scatter plots of VisR τ estimates before and after correction versus true material τ values for the case of acoustically tracked FEM displacements. Recall from section III.D that unique corrections functions were generated to account for the additional error introduced by acoustic displacement underestimation, so (11–12) and (13–14) were applied to correct VisR τ estimates at 25 mm and 30 mm, respectively. As Table 1 shows, for both depths, estimated VisR τ values were statistically significantly larger than true material τ values before correction ($p<0.001$), and median (inter-quartile range) percent error was 372.7 (447.3)% and 583.0 (600.1)% at 25 mm and 30 mm, respectively. After correction, VisR τ values did not statistically differ from true material τ values ($p=0.96$ and 0.85 for 25 and 30 mm measurements, respectively). Further, median (inter-quartile range) percent error was reduced to −5.4 (39.3)% for 25 mm and −12.3 (73.3)% for 30 mm. Note that after correction, error in VisR τ estimates derived from acoustically tracked displacements was comparable to that derived from raw FEM displacements.

D. Inertial Compensation with Volumetric ARF Excitation In Vivo

Parametric images of uncorrected and corrected VisR τ estimates made in the rectus femoris muscle of an adult female with no known neuromuscular disorders are displayed in Fig. 10. Prior to correction for inertia and displacement underestimation (panel a), the median (std) VisR τ value in the depth range of 23 to 33 mm was 1.840 (0.134) ms. After correction using (11–14), the median (std) VisR τ value in the depth range of 23 to 33 mm was reduced to 0.675 (0.210) ms. This corrected median VisR τ value is consistent with previous SDUV measures of viscoelasticity made in bovine muscle in the matched cross-sectional orientation: SDUV viscosity / SDUV elasticity = 5.7 Pa·s /12 kPa = 0.475 ms [10].

V. Discussion

This work utilized FEM models to simulate viscoelastic dynamics using both single point and volumetric forces. It is important to note that these FEM models simulate each element in the mesh as a distributed network of masses, springs, and dampers in three dimensions [24]. The interconnected nature of the elements creates complex behavior and multiple degrees of freedom in the simulated environment that, in general, cannot be directly recapitulated using a SDF model, such as the Voigt or MSD model [15]. However, in the case of an idealized point force, as described in sections IV.A, the MDF FEM simulation approximately reduces to a SDF system at the focal point. In this case, the accuracy of VisR measures of τ is predominantly dependent on the relevance of the SDF viscoelastic model chosen to describe the response of the material.

The Voigt model assumes a massless material. This assumption was valid for focused point force excitations when a density of 0.05 g/cm^3 was used for FEM modeled materials. In Fig. 5(a) there is very little observable difference between the FEM displacement and the Voigt predicted displacement, and as shown in Fig. 6(a), the Voigt model accurately estimated τ values in all 15 viscoelastic materials. However, the Voigt model did not accurately estimate τ values when density was increased to 1.0 g/cm^3. The effects of inertia on the dynamic response of the material, as can be seen in Fig. 5(b), manifest as a delay in response to the initiation and cessation of force. The Voigt model does not account for the change in the displacement profile due to inertia; the delay in the time for the material to reach its peak and to recover is attributed to increase in material viscosity and/or a decrease in the stiffness of the material. This is reflected in an increase in estimated τ relative to the true value (Fig. 6(c)). The fact that the Voigt model could only generate τ values that were not statistically different from the real values when mass density was below 0.7 g/cm^3 (Fig. 7) limits its use for imaging soft tissue, as the density of these tissues is between 0.9–1.1 g/cm^3. Conversely, the MSD model, which involves an inertial component, does compensate for changes in the density of the medium. The MSD model generated τ estimates that were consistent with the actual τ of the material over the full range of investigated densities when using a point force to generate displacement (Fig. 6(d)).

While the MSD model enables VisR τ measurement by accounting for inertia in the case of an idealized point load, the SDF assumption fails in the case of a volumetric load that induces complex, three-dimensional system inertia. Thus VisR significantly overestimated τ, both in the simplified case of no acoustic tracking (Fig. 8(a,c)) and in the case of acoustic displacement underestimation (Fig. 9(a,c)). These results are in agreement with those previously reported by Zhao and Pelegri, which showed that larger ARF focal regions increased estimation error using SDF models [15].

In order for VisR to be quantitative with the use of volumetric ARF excitations, empirically determined, depth-dependent error correction functions were applied to raw τ estimates. After correction (Fig. 8(b, d) and Fig. 9(b, d)), median percent error in corrected VisR τ estimates was substantially reduced to approximately −10%. The mathematical justification for the form of the error correction functions is currently unknown, but it stands to reason that the correction is a function of material properties (raw τ and/or ω) and excitation

geometry (focal position and configuration) based on the findings of Zhao and Pelegri that error in τ estimation using SDF models is both materially and geometrically dependent [15].

VisR with τ correction was demonstrated for proof of clinical feasibility in normal human rectus femoris muscle, *in vivo* (Fig. 10). After correction, mean VisR τ estimates in the depth range of 23 to 33 mm were reduced to a value consistent with that previously reported using SDUV measures of viscosity and elasticity in bovine muscle, suggesting that VisR with error correction may be relevant to measuring τ in muscle, *in vivo*. This will be explored further in future investigations. Of particular relevance to VisR applications in muscle (and other tissues) are heterogeneity and anisotropy. Zhao and Pelegri showed that the displacement response of the focal region is impacted by local heterogeneity, which degrades the effectiveness of the SDF simplification, and we predict that anisotropy will have a similar effect. Moreover, for the clinical muscle examples presented herein, the error correction functions were derived from FEM models of homogeneous, isotropic viscoelastic media. The pertinence of these corrections to heterogeneous, anisotropic tissue is yet to be determined.

Another important consideration in the application of error correction functions is the depth range over which a given correction is meaningful. The depth dependence of error correction functions is most likely attributable to variations in the spatial extent and magnitude of the volumetric ARF excitations with depth, suggesting that the ARF focal depth and configuration are impactful. In this investigation, we derived two correction functions separated by 5 mm for VisR imaging over a 10 mm axial range centered at the focal depth of 25 mm for an F/1.5 ARF focal configuration. Optimizing the axial spacing of error correction functions, such that error in VisR τ estimates is minimized while maximizing computational efficiency, and evaluating the impact of ARF focal depth and configuration on error correction performance will be investigated in the future. While we note that unique error correction functions are likely to be needed for different ARF focal depths and configurations, mostly because altering the ARF parameters will change the associated complex system inertia, defining and optimizing the robustness of a given correction function to variations in ARF excitations is the topic of future investigation.

VI. Conclusions

VisR, an ARF-based viscoelastic imaging method that estimates the ratio of viscosity to elasticity (τ) in viscoelastic materials, is herein evaluated for its potential to quantify the viscoelastic properties of tissue. VisR τ estimates derived by fitting displacements to the MSD, as opposed to Voigt, model accurately described true material τ in FE simulated viscoelastic materials when idealized point force excitations were applied to materials with density comparable to that of human soft tissue. These data highlight the need to account for inertia due to tissue mass in VisR imaging. However, complex three-dimensional system inertia and acoustic displacement underestimation become confounding issues when using volumetric ARF excitations and acoustic displacement tracking. Under such circumstances, the MSD model did not sufficiently account for the multiple degrees of freedom in the system dynamics. Therefore, empirically determined error correction functions were derived to reduce error in VisR τ estimates. With correction, median percent error in VisR τ

estimates, derived from raw FEM as well as acoustically tracked displacements, was approximately −10%. In application to *in vivo* imaging in muscle, corrected VisR τ estimates were consistent with those previously measured by SDUV, suggesting VisR's potential relevance to quantifying viscoelastic properties clinically.

Acknowledgments

We thank the staff of ITS Research Computing (University of North Carolina at Chapel Hill) for their resources and support in using the KillDevil supercomputing cluster. We also thank Siemens Healthcare, Ultrasound Business Unit, for technical support.

References

1. Nightingale K, Rouze N, Rosenzweig S, Wang M, Abdelmalek M, Guy C, Palmeri M. Derivation and analysis of viscoelastic properties in human liver: impact of frequency on fibrosis and steatosis staging. IEEE Trans. Ultrason. Ferroelectr. Freq. Control. 2015; 62(1):165–175. [PubMed: 25585400]
2. Deffieux T, Montaldo G, Tanter M, Fink M. Shear wave spectroscopy for in vivo quantification of human soft tissues visco-elasticity. IEEE Trans. Med. Imaging. 2009; 28(3):313–322. [PubMed: 19244004]
3. Chen S, Sanchez W, Callstrom M. Assessment of liver viscoelasticity by using shear waves induced by ultrasound radiation force. Radiology. 2013; 266(3):964–970. [PubMed: 23220900]
4. Salameh N, Peeters F, Sinkus R, Abarca-Quinones J, Annet L, ter Beek LC, Leclercq I, Van Beers BE. Hepatic viscoelastic parameters measured with MR elastography: Correlations with quantitative analysis of liver fibrosis in the rat. J Magn. Reson. Imaging. 2007 Oct.26(4):956–962. [PubMed: 17896384]
5. Qiu Y, Sridhar M, Tsou JK, Lindfors KK, Insana MF. Ultrasonic Viscoelasticity Imaging of Nonpalpable Breast Tumors. Acad. Radiol. 2008 Dec.15(12):1526–1533. [PubMed: 19000869]
6. Sinkus R, Tanter M, Catheline S, Lorenzen J, Kuhl C, Sondermann E, Fink M. Imaging anisotropic and viscous properties of breast tissue by magnetic resonance-elastography. Magn. Reson. Med. 2005; 53(2):372–387. [PubMed: 15678538]
7. Hoyt K, Kneezel T, Castaneda B, Parker KJ. Quantitative sonoelastography for the in vivo assessment of skeletal muscle viscoelasticity. Phys. Med. Biol. 2008 Aug.53(15):4063–4080. [PubMed: 18612176]
8. Gennisson JL, Deffieux T, Macé E, Montaldo G, Fink M, Tanter M. Viscoelastic and anisotropic mechanical properties of in vivo muscle tissue assessed by supersonic shear imaging. Ultrasound Med. Biol. 2010; 36(5):789–801. [PubMed: 20420970]
9. Selzo MR, Gallippi CM. Viscoelastic response (VisR) imaging for assessment of viscoelasticity in voigt materials. IEEE Trans. Ultrason. Ferroelectr. Freq. Control. 2013; 60(12):2488–2500. [PubMed: 24297015]
10. Chen SG, Urban MW, Pislaru C, Kinnick R, Zheng Y, Yao AP, Greenleaf JF. Shearwave Dispersion Ultrasound Vibrometry (SDUV) for Measuring Tissue Elasticity and Viscosity. IEEE Trans. Ultrason. Ferroelectr. Freq. Control. 2009; 56(1):55–62. [PubMed: 19213632]
11. Bercoff J, Tanter M, Muller M, Fink M. The role of viscosity in the impulse diffraction field of elastic waves induced by the acoustic radiation force. IEEE Trans. Ultrason. Ferroelectr. Freq. Control. 2004; 51(11):1523–1536. [PubMed: 15600098]
12. Sarvazyan AP, Rudenko OV, Swanson SD, Fowlkes JB, Emelianov SY. Shear wave elasticity imaging: a new ultrasonic technology of medical diagnostics. Ultrasound Med. Biol. 1998 Nov. 24(9):1419–1435. [PubMed: 10385964]
13. Viola F, Walker WF. Radiation force imaging of viscoelastic properties with reduced artifacts. IEEE Trans. Ultrason. Ferroelectr. Freq. Control. 2003; 50(6):736–742. [PubMed: 12839188]
14. Mauldin FW, Haider Ma, Loboa EG, Behler RH, Euliss LE, Pfeiler TW, Gallippi CM. Monitored steady-state excitation and recovery (MSSER) radiation force imaging using viscoelastic models. IEEE Trans. Ultrason. Ferroelectr. Freq. Control. 2008; 55(7):1597–1610. [PubMed: 18986950]

15. Zhao X, Pelegri Aa. Dynamic Simulation of Viscoelastic Soft Tissue in Acoustic Radiation Force Creep Imaging. J Biomech. Eng. 2014 Jul.136:094502. no. September 2014. [PubMed: 24975997]
16. Amador C, Urban MW, Chen S, Greenleaf JF. Loss tangent and complex modulus estimated by acoustic radiation force creep and shear wave dispersion. Phys Med Biol. 2012; 57(5):1263–1282. [PubMed: 22345425]
17. Isaacs, A. A Dictionary of Physics. Sixth. New York: Oxford University Press; 2009.
18. Fung, Y. Biomechanics: Mechanical Properties of Living Tissue. New York: Springer; 1993.
19. Christensen, D. Ultrasonic Bioinstrumentation. New York: John Wiley & Sons; 1988.
20. Palmeri ML, McAleavey SA, Fong KL, Trahey GE, Nightingale KR. Dynamic mechanical response of elastic spherical inclusions to impulsive acoustic radiation force excitation. IEEE Trans Ultrason Ferroelectr Freq Control. 2006; 53(11):2065–2079. [PubMed: 17091842]
21. Palmeri ML, McAleavey SA, Trahey GE, Nightingale KR. Ultrasonic tracking of acoustic radiation force-induced displacements in homogeneous media. IEEE Trans. Ultrason. Ferroelectr. Freq. Control. 2006 Jul.53(7):1300–1313. [PubMed: 16889337]
22. Czernuszewicz TJ, Streeter JE, Dayton Pa, Gallippi CM. Experimental validation of displacement underestimation in ARFI ultrasound. Ultrason. Imaging. 2013; 35(3):196–213. [PubMed: 23858054]
23. Wu C, Han Z, Wang S, Li J, Singh M, Liu C-h, Aglyamov S, Emelianov S, Manns F, Larin KV. Assessing Age-Related Changes in the Biomechanical Properties of Rabbit Lens Using a Coaligned Ultrasound and Optical Coherence Elastography System. Invest. Ophthalmol. Vis. Sci. 2015; 56(2):1292–1300. [PubMed: 25613945]
24. Takács, G.; Rohal'-Ilkiv, B. Model Predictive Vibration Control. London: Springer London; 2012. Basics of Vibration Dynamics.
25. Palmeri ML, Sharma AC, Bouchard RR, Nightingale RW, Nightingale KR. A finite-element method model of soft tissue response to impulsive acoustic radiation force. IEEE Trans. Ultrason. Ferroelectr. Freq. Control. 2005; 52(10):1699–1712. [PubMed: 16382621]
26. Basu U. Explicit finite element perfectly matched layer for transient three-dimensional elastic waves. Int. J. Numer. Methods Eng. 2009; 77(2):151–176.
27. Lagarias JC, Reeds JA, Wright MH, Wright PE. Convergence Properties of the Nelder--Mead Simplex Method in Low Dimensions. SIAM J. Optim. 1998 Jan.9(1):112–147.
28. Jensen JA, Svendsen NB. Calculation of pressure fields from arbitrarily shaped, apodized, and excited ultrasound transducers. IEEE Trans. Ultrason. Ferroelectr. Freq. Control. 1992; 39:262–267. [PubMed: 18263145]
29. Nightingale KR, Kornguth PJ, Trahey GE. The use of acoustic streaming in breast lesion diagnosis: a clinical study. Ultrasound Med. Biol. 1999; 25:75–87. [PubMed: 10048804]
30. Nightingale K, Soo MS, Nightingale R, Trahey G. Acoustic radiation force impulse imaging: in vivo demonstration of clinical feasibility. Ultrasound Med. Biol. 2002; 28(2):227–235. [PubMed: 11937286]
31. Pinton GF, Dahl JJ, Trahey GE. Rapid tracking of small displacements with ultrasound. IEEE Trans. Ultrason. Ferroelectr. Freq. Control. 2006 Jun.53(6):1103–1117. [PubMed: 16846143]
32. Arlot S, Celisse A. A survey of cross-validation procedures for model selection. Stat. Surv. 2010; 4:40–79.
33. Giannantonio DM, Dumont DM, Trahey GE, Byram BC. Comparison of Physiological Motion Filters for In Vivo Cardiac ARFI. Ultrason. Imaging. 2011 Apr.33(2):89–108. [PubMed: 21710825]

Biographies

Mallory R. Selzo received a B.S. degree in Computer Engineering from the University of Washington in 2008 and a Ph.D. from the Joint Department of Biomedical Engineering at the University of North Carolina and North Carolina State University in 2015. She is currently a Senior Systems Engineer in the Advanced Development group at Siemens Healthcare in Issaquah, WA.

Christopher J. Moore was born in Newark, OH in 1989. He received his B.F.A in production design and his B.S. in electrical engineering from Ohio University in 2012 and 2013, respectively. He is currently pursuing a Ph. D. degree in the Department of Electrical and Computer Engineering at North Carolina State University. His research interests include viscoelasticity imaging methods and muscle imaging.

Md Murad Hossain earned his B.Sc and M. Sc degree in electrical engineering from the Islamic University of Technology, Bangladesh and George Mason University, USA in 2009 and 2014, respectively. He is currently pursuing a Ph.D. degree in the joint Department of Biomedical Engineering at the University of North Carolina – Chapel Hill and North Carolina State University. His research interests include acoustic radiation force imaging and medical signal processing.

Mark L. Palmeri received his B.S. degree in Biomedical and Electrical Engineering from Duke University, Durham, NC, in 2000. He was a James B. Duke graduate fellow and received his Ph.D. degree in Biomedical Engineering from Duke University in 2005 and his M.D. degree from the Duke University School of Medicine in 2007. He is currently an

Associate Research Professor in Biomedical Engineering and Anesthesiology at Duke University. He is an Associate Editor for Ultrasound in Medicine and Biology and IEEE Transactions in Medical Imaging. He serves as a sub-committee co-chair for the RSNA Quantitative Imaging Biomarker Alliance (QIBA) ultrasound shear wave speed imaging committee. His research interests include acoustic radiation force, shear wave elasticity imaging, finite element analysis, medical image and signal processing, and medical device design.

Caterina M. Gallippi earned a B.S.E. degree in electrical engineering and a certificate in engineering biology from Princeton University in 1998. She completed her Ph.D. degree in biomedical engineering at Duke University in 2003 with a focus on ultrasonic imaging. She is currently an associate professor in the joint Department of Biomedical Engineering at the University of North Carolina - Chapel Hill and North Carolina State University. Her research interests include radiation force imaging, adaptive signal filtering, multidimensional motion tracking, and magneto-motive ultrasound.

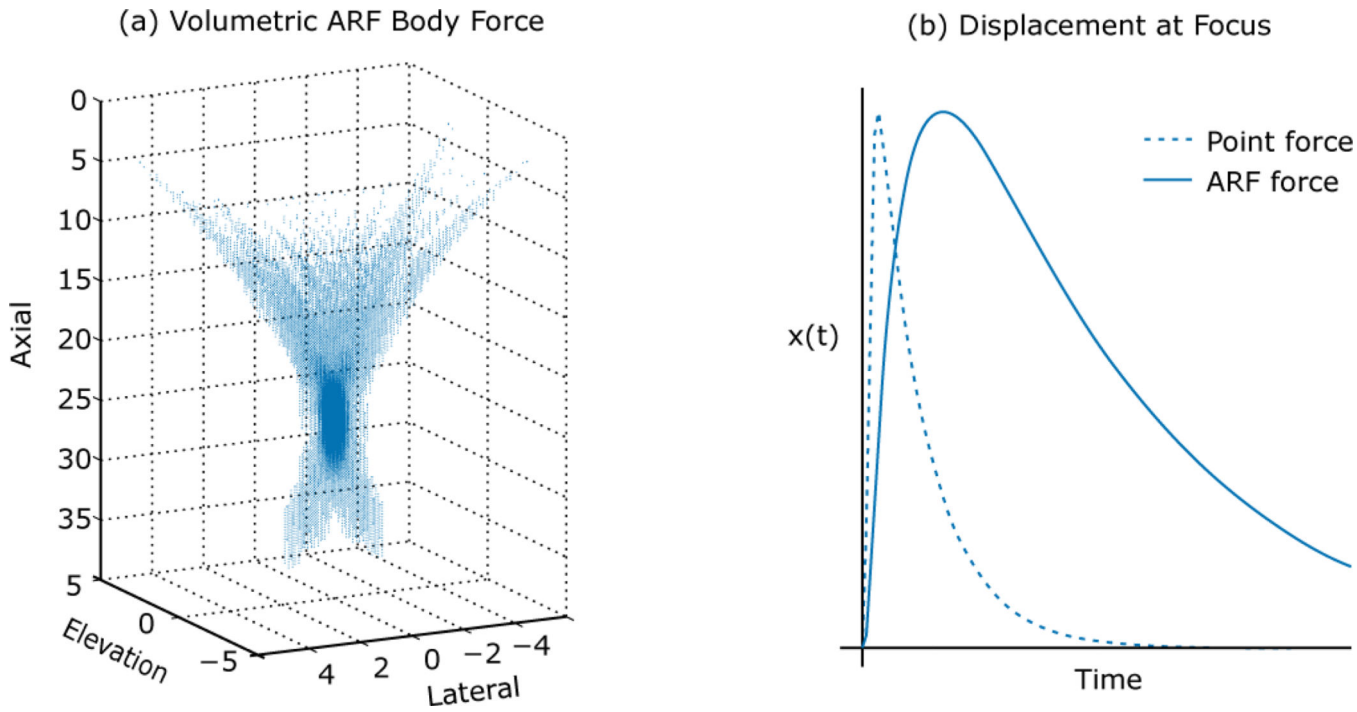

Fig. 1.

(a) Spatial distribution of force using a volumetric ARF body force. (b) Axial displacement at focus induced by a single point force (dashed) and induced by a volumetric ARF body force (solid).

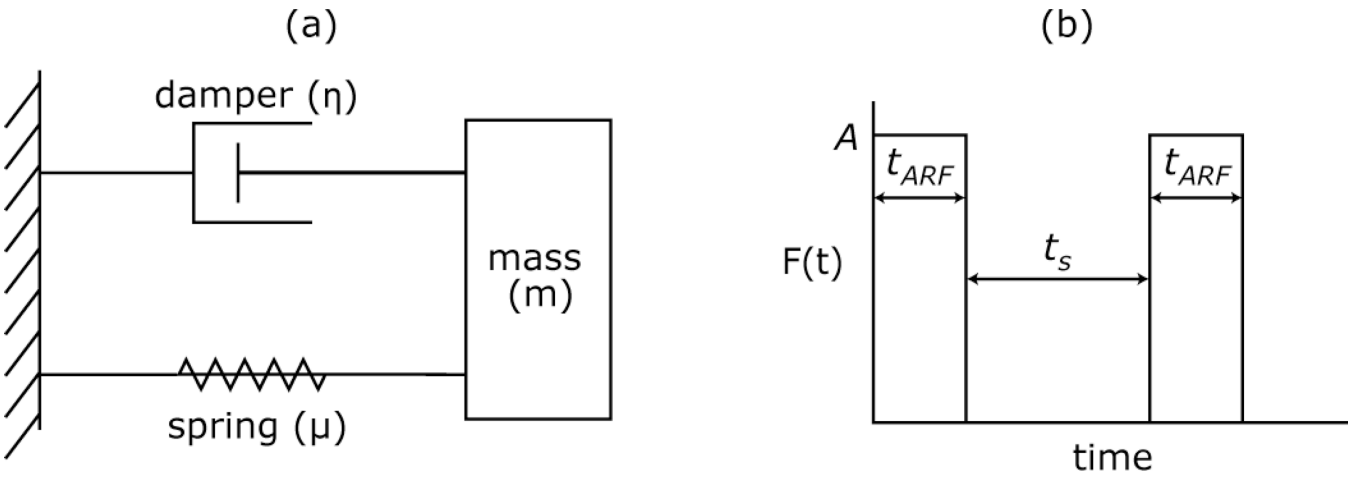

Fig. 2.

(a) A schematic of the mass-spring-damper (MSD) model and (b) a graphical illustration of the forcing function input

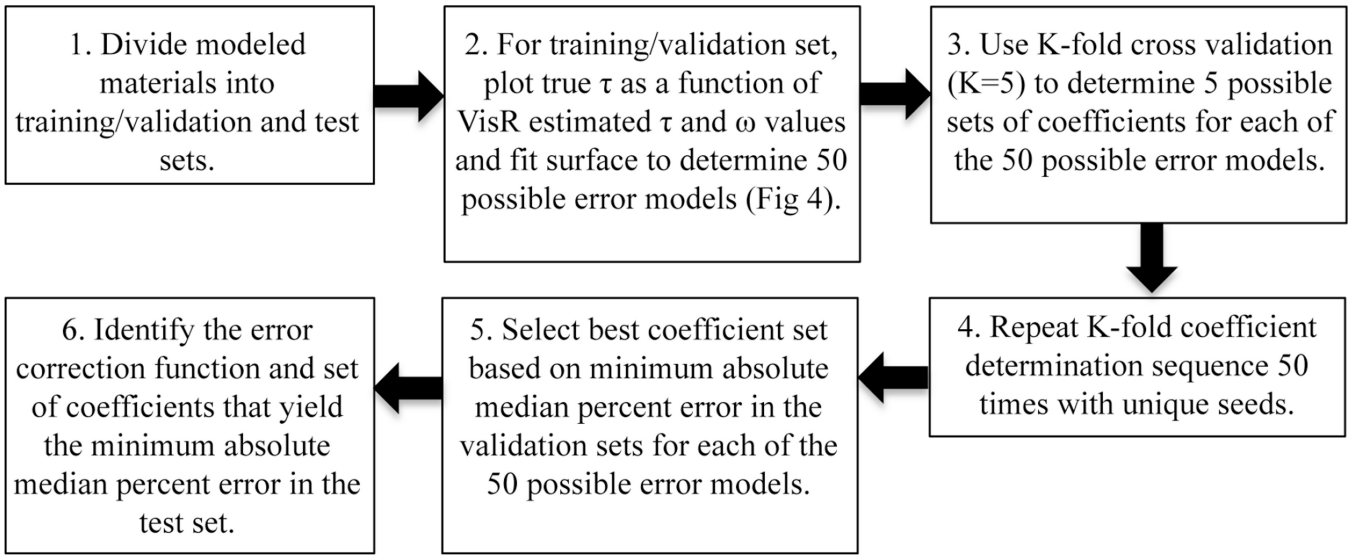

Fig. 3.
Flow chart representing the methods of error correction function determination for VisR **τ** estimation.

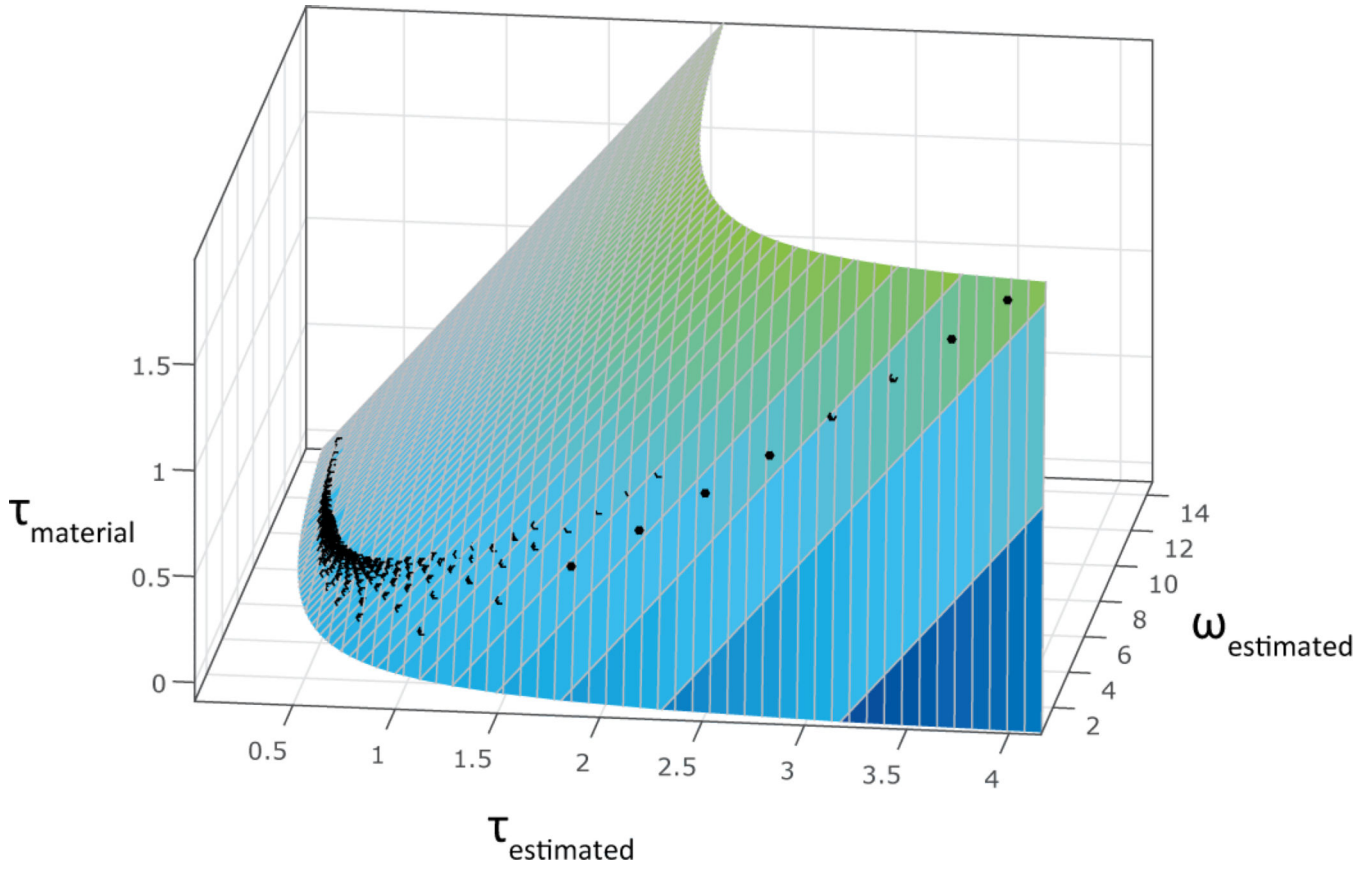

Fig. 4.

True material τ plotted as a function of the estimated τ and ω material parameters. The resulting 3-dimensional surface fits the error data well, $R^2 = 0.999$.

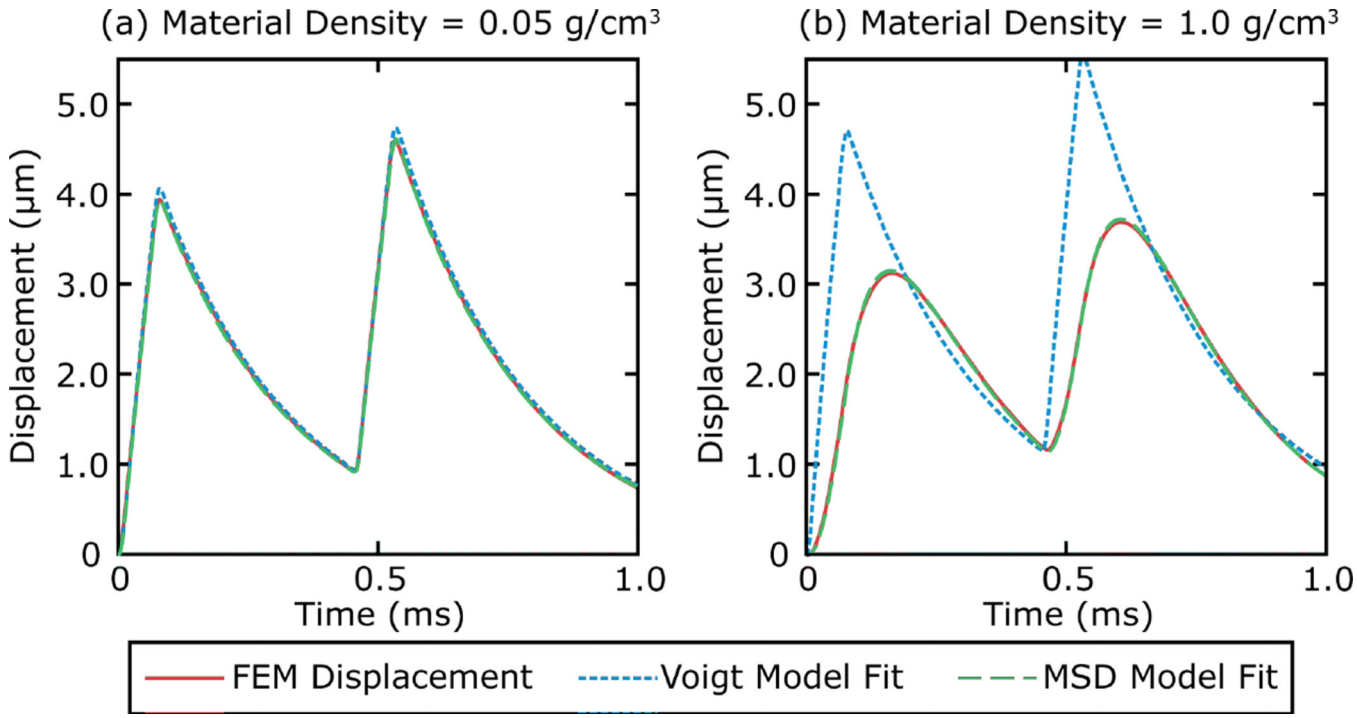

Fig. 5.

Simulated displacement profiles (red, solid) in a 20 kPa, 5 Pa·s material with a mass density of (a) 0.05 g/cm3 and (b) 1.0 g/cm3 and the predicted displacement using the Voigt (blue or dotted) and MSD (green or dashed) models.

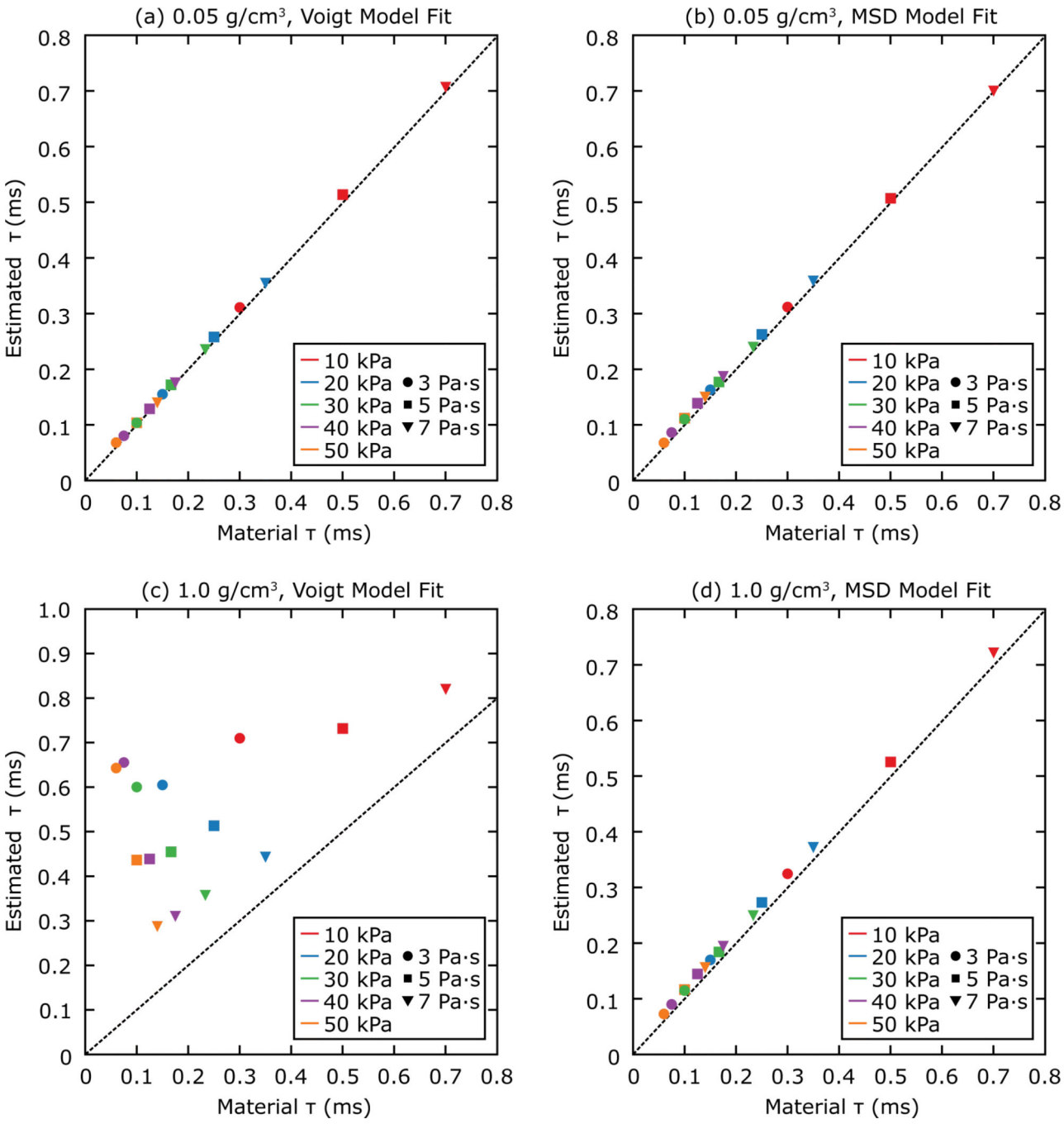

Fig.6.

Scatter plots of VisR **τ** estimates versus the simulated material **τ** for the 15 viscoelastic materials with a density of (top row) 0.05 g/cm3 or (bottom row) 1.0 g/cm3. The elasticity of the material is indicated by color and viscosity is indicated by symbol. The dashed black line indicates the line of equality. Estimates of **τ** in the 0.05 g/cm3 dense materials were consistent with the material **τ** ($p > 0.05$, Wilcoxon two-sample test) using both the Voigt (a) and MSD (b) models. In the 1.0 g/cm3 dense materials, **τ** estimations were statistically

different from the material $\boldsymbol{\tau}$ when made using the Voigt (c) model but consistent with the material $\boldsymbol{\tau}$ when using the MSD model (d).

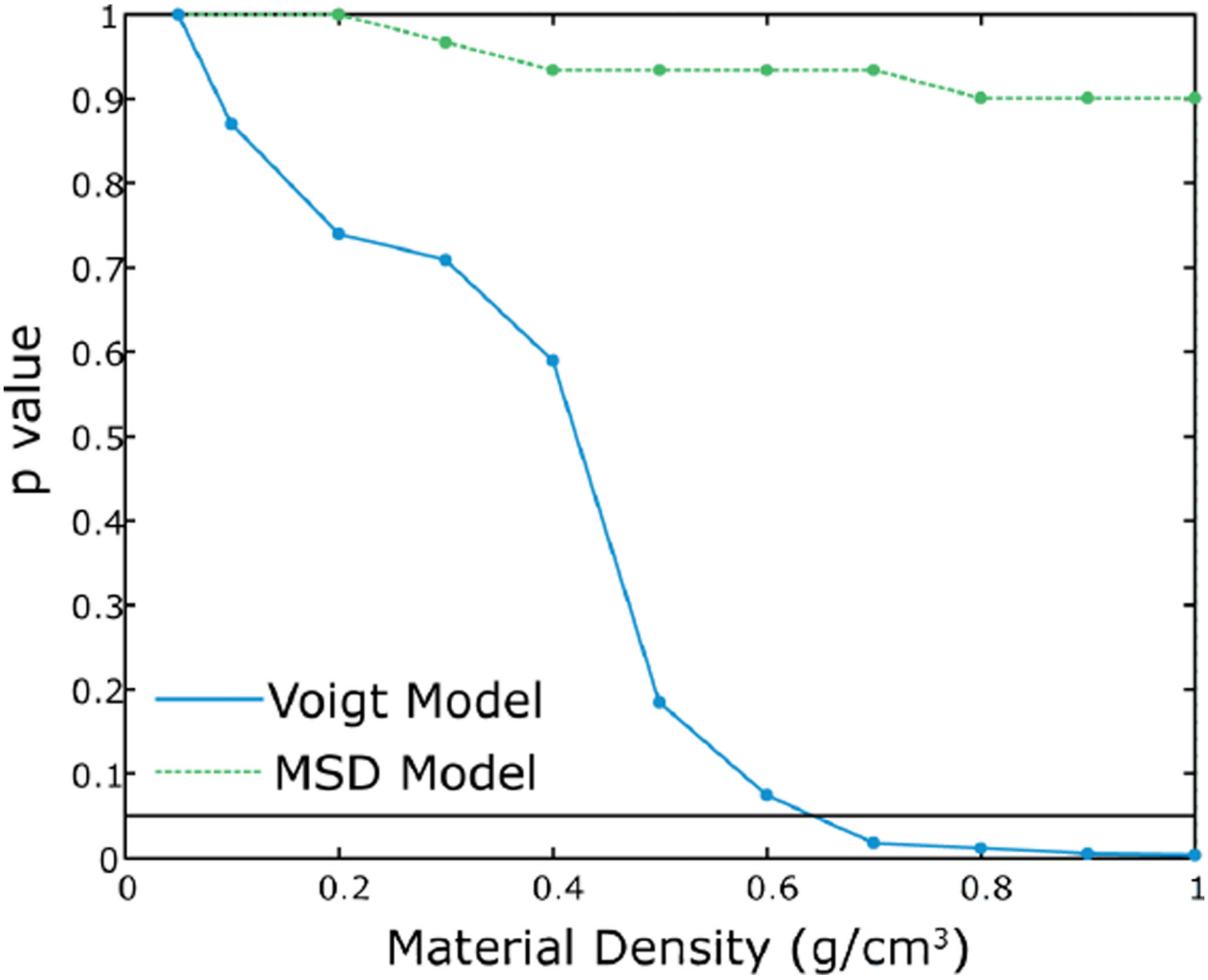

Fig. 7.

Wilcoxon rank-sum p-values testing the null hypothesis that the modeled material and VisR-derived τ values are the same versus material density for the Voigt (blue) and MSD (green) model fits. The black line represents statistical significance at the 0.05 level. Voigt model derived τ estimates were statistically significantly different from the real τ of the materials for density > 0.6 g/cm3. Estimates of τ generated using the MSD model were consistent with the material τ values at all densities.

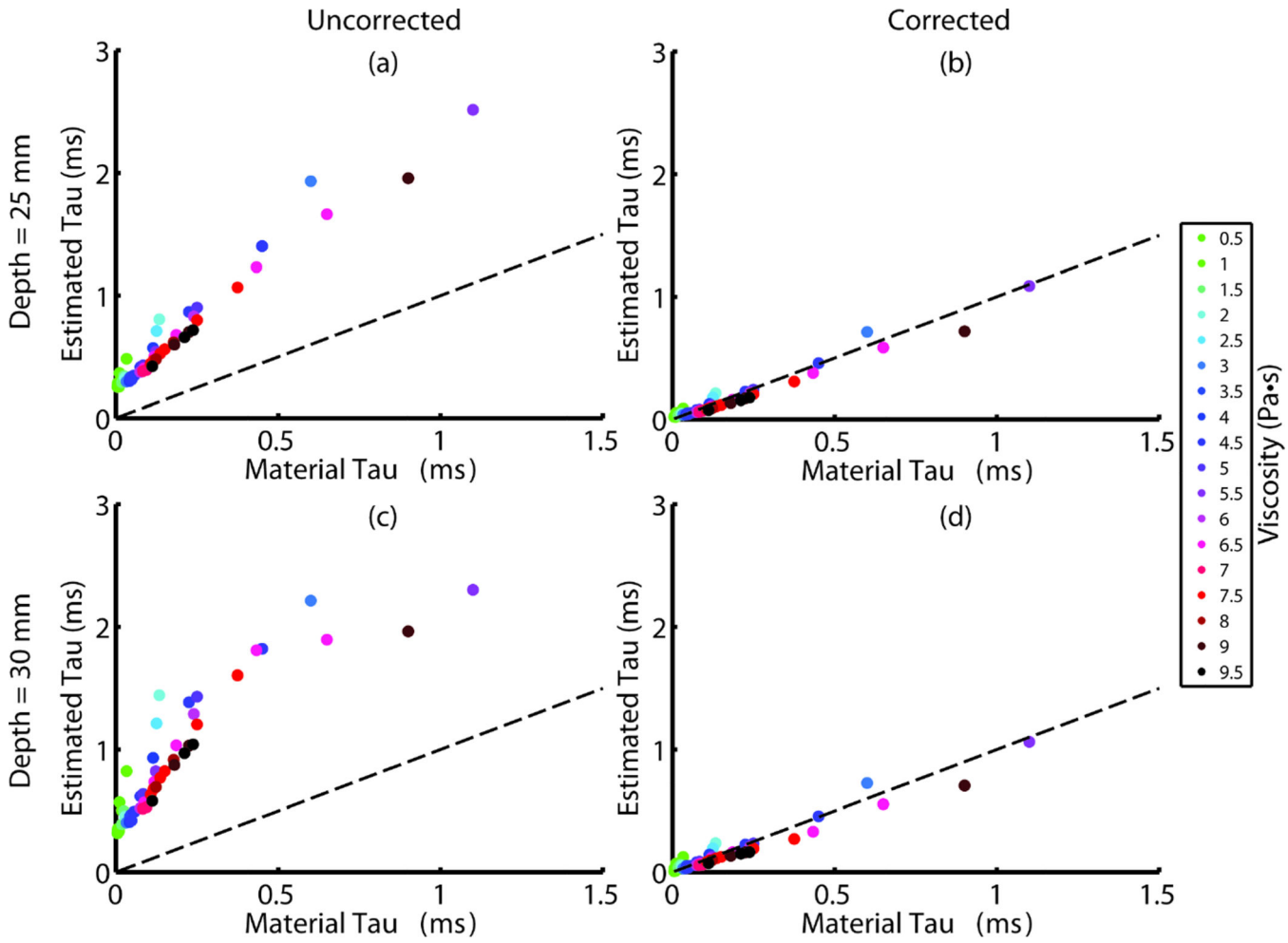

Fig. 8.

Scatter plots of (left column) uncorrected and (right column) inertia-corrected VisR τ estimates from raw FE displacements in the 50 simulated viscoelastic test materials versus the true τ of the material. Results are for measurements at depth positions of 25 (top row) and 30 mm (bottom row) given 25 mm ARF excitation and tracking line focal depths. The viscosity of the material is indicated by color and the dashed black line indicates the line of equality. FE = finite element.

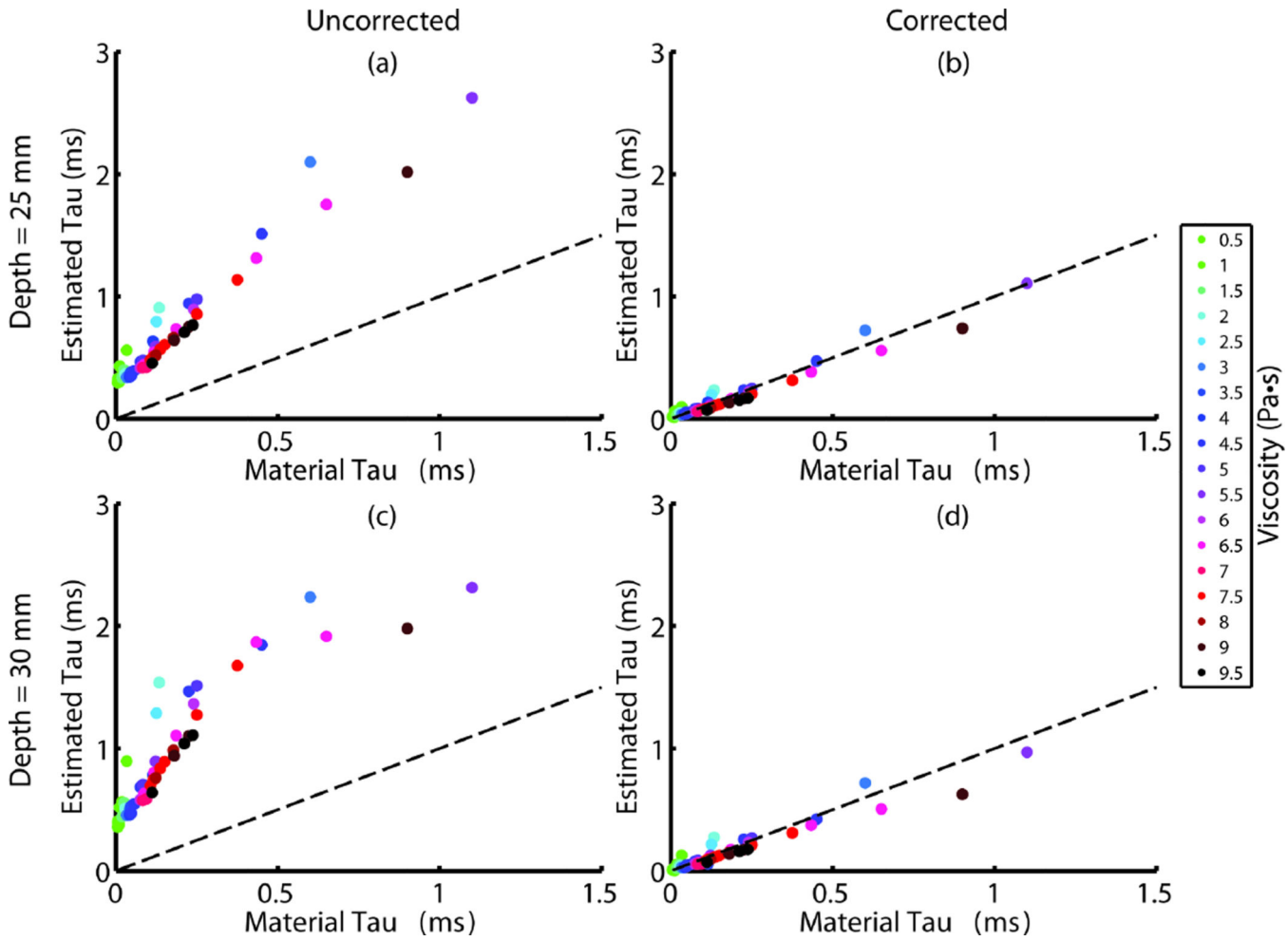

Fig. 9.

Scatter plots of (left column) uncorrected VisR τ, and (right column) VisR τ after correction for both inertia and displacement-underestimation. These plots show VisR τ results from simulated acoustic tracking of FE displacements in 50 simulated viscoelastic test materials versus the true τ of the material. Results are for measurements at depth positions of 25 (top row) and 30 mm (bottom row) given 25 mm ARF excitation and tracking line focal depths. The viscosity of the material is indicated by color and the dashed black line indicates the line of equality. FE = finite element.

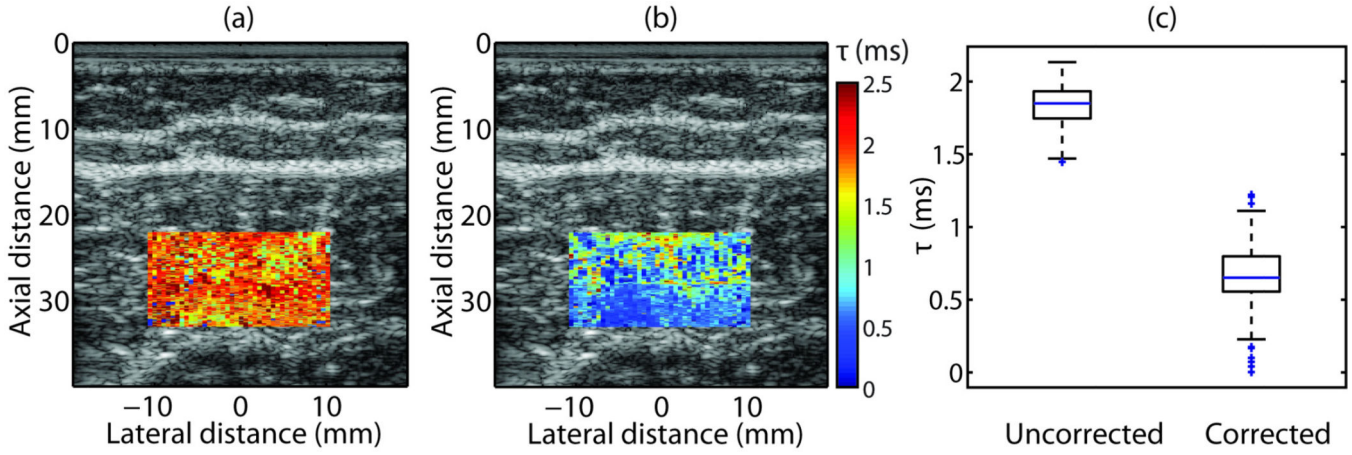

Fig. 10.

In vivo comparison of parametric VisR τ images both (a) uncorrected and (b) after correction for both inertia and displacement underestimation, in human rectus femoris muscle. (c) Prior to correction, median and (IQR) of raw VisR τ values are 1.850 (0.19) ms, and after correction, median and IQR of corrected VisR τ values are 0.651 (0.242) ms.

TABLE I

Error in Uncorrected and Corrected Visr τ Estimates in FE Simulation

	FEM				Ultrasonic Tracking			
	Before Correction		After Correction		Before Correction		After Correction	
	25 mm	30 mm	25 mm	30 mm	25 mm	30 mm	25 mm	30 mm
Median Error (ms)	0.371	0.594	−0.010	−0.012	0.423	0.654	−0.003	−0.012
IQR Error (ms)	0.250	0.519	0.029	0.040	0.270	0.533	0.042	0.040
Median Error (%)	333.715	525.732	−9.344	−9.588	372.715	583.010	−5.441	−12.280
IQR Error (%)	375.776	523.530	25.717	42.670	447.321	600.080	39.317	37.300
P-value	<0.001	<0.001	0.95	0.94	<0.001	<0.001	0.96	0.85